Supplementary Information

A. Constraining the size of the pallasite parent body

Both Tarduno et al. (2012) and Bryson et al. (2015) demonstrate that for the cooling rates and paleomagnetic fields experienced by the Esquel and the Imilac pallasites, the pallasite parent body must have a radius similar to 200 km. They rule out a 100 km radius body, as this would have cooled too quickly, solidifying the core completely before the pallasites could become magnetised. A 300 km body is ruled out by Bryson et al. as the core would not have begun to solidify when the Esquel and Imilac experienced a magnetic field, and the field is too intense to be generated by a very weak thermal dynamo field. A 600 km body is ruled out, since this would place the pallasites in the insulating megaregolith layer, in which case signs of shock, and other silicate minerals would be expected.

We have calculated the timing of magnetisation and depth of the pallasites in a body of radius 150 km and 250 km (Table 1). For a 150 km radius body, the Imilac and Esquel would have become magnetised after complete core solidification. A radius of 250 km is possible, however it has little affect on the timing of magnetisation, so does not effect our reported results.

	Marjalahti and Brenham		Imilac and Esquel	
Pallasite Parent Body Radius	Depth in parent body	Paleomagnetic signal age	Depth in parent body	Paleomagnetic signal age
150 km	27 km	102 Ma after accretion	45 km	after complete core solidification
200 km	22 km	103 Ma after accretion	40 km	190-237 Ma after accretion
250 km	18 km	104 Ma after accretion	35 km	185-246 Ma after accretion

Table 1: Cooling models for the pallasite parent body have been considered for radii 150 km, 200 km and 250 km. The average depth of the Brenham and Marjalahti and the Imilac and Esquel haven been calculated for each radius. The timing of paleomagnetic acquisition has also been shown, where this is taken to be the time at which the pallasites cool through 320 °C, the ordering temperature of tetrataenite. A pallasite parent body with radius 150 km cools too quickly; Imilac and Esquel would not have become magnetised until after core solidification was complete. For radii of 200 km and 250 km, results are similar, suggesting small changes in the size of parent body do not effect our interpretations.

B. Bootstrapping Technique

Figure 1 shows a probability density function and its integral, representing the distribution of XMCD values measured experimentally in the cloudy zone. By randomly resampling the integrated probability, a statistically significant distribution of the mean XMCD value can be generated. This is essential in order to constrain the likelihood of the Marjalahti and Brenham having experienced very weak applied fields.

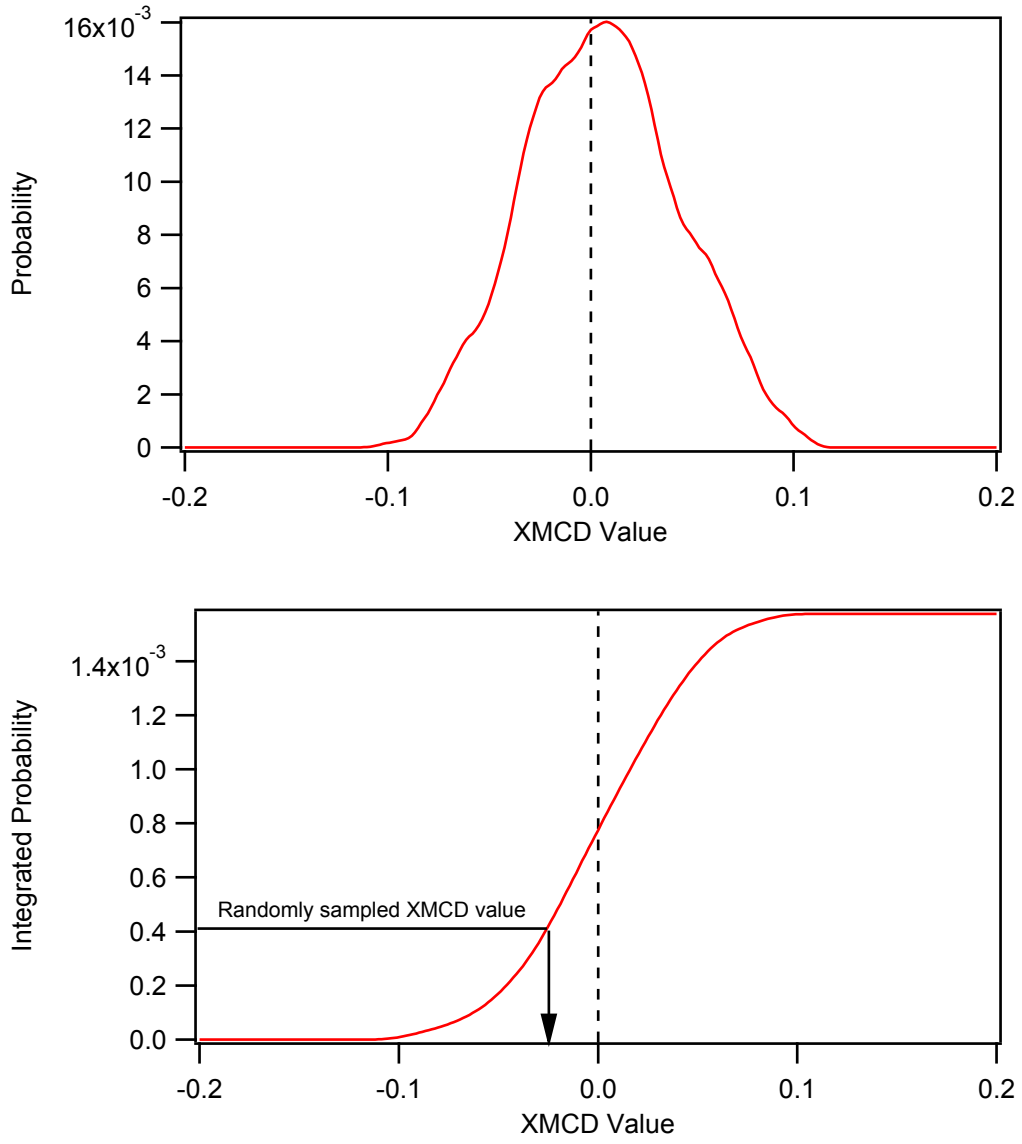

Figure 1: Histograms of XMCD value are converted to probability density functions. The curve is then integrated, and plotted against XMCD value. This curve is then randomly sampled to generate representative distributions. This is repeated 1000 times, a process known as bootstrapping, in order to calculate the mean and of each distribution to >95 % confidence.

C. Qualitative comparison of pixel intensity histograms

The validity of XMCD as a method to quantify the paleomagnetic fields experienced by the four pallasites (Brenham, Marjalahti, Imilac and Esquel) can be investigated by qualitative comparison of the histograms of pixel intensity (Figure2). We find that the calculated paleomagnetic field values (Table 2) are in very good agreement with the symmetry and offset of each histogram. For paleomagnetic fields >100 μT, the histograms show significant asymmetry, with the peak of the histogram significantly offset from zero indicating a strong bias in XMCD value. For paleomagnetic fields $<$ 100 μT, the histograms have a more symmetric distribution, and the offset of the peak from zero depends on the strength of the field; the Esquel shows a notable offset for regions 3 – 5, whereas there is negligible offset from zero for region 6, as well as the Marjalahti and Brenham, all of which experienced a paleomagnetic field $<$ 10 μT.

We also show that our results are reproducible and consistent. The Brenham has been measured twice, in two separate experiments. The orientation and regions of interest imaged using XMCD and X-PEEM in each case are random and unrelated. The histograms of pixel intensity from both experiments show symmetric distributions with very small offsets from zero. Small variations in the widths of the histograms may be due to a small difference in the Ni content of the two regions examined, and are also influenced by the image resolution and degree of island clustering.

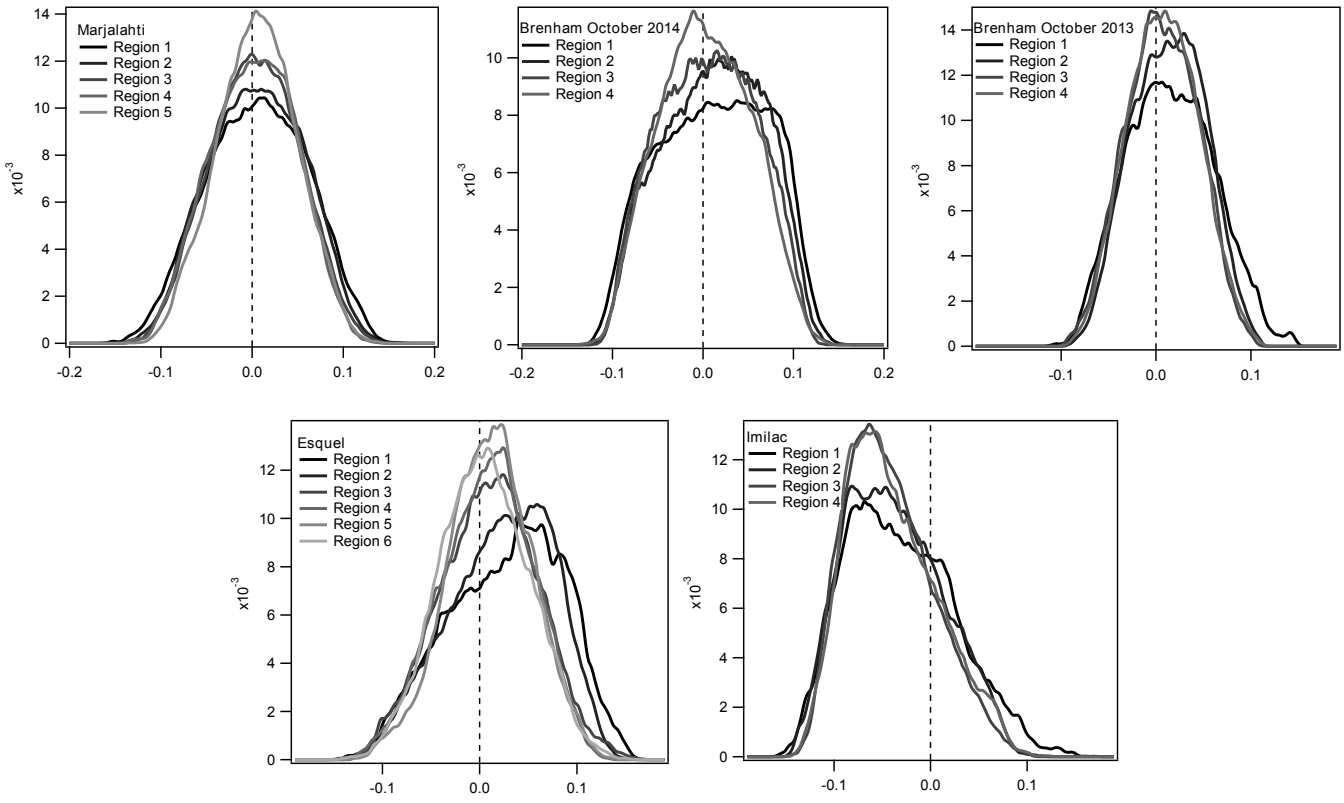

Figure 2: A comparison of the histograms of pixel intensity for the Marjalahti, Brenham, Imilac and Esquel. The Marjalahti shows a symmetric distribution, slightly offset from zero. The Brenham has been measured twice in two orientations, during two separate experiments. In both cases, the distribution is symmetric with a small offset from zero. This demonstrates the ability of XMCD to reproduce results and provide reliable information about magnetisation of the sample. The Esquel has a very asymmetric distribution for the first two regions, and then becomes more symmetric with a smaller offset from zero. The Imilac shows an asymmetric distribution and strong offset from zero for all regions. These qualitative histogram observations are consistent with the magnetic field values calculated for each region of the four pallasites; asymmetric distributions with a large offset are consistent with large fields, > 100 μT, whilst small offsets and symmetric distributions correspond to much smaller fields < 10 μT.

	Average calculated field value (μT)			
Region	**Marjalahti**	**Brenham**	**Imilac**	**Esquel**
1	5.0 ± 1.4	4 ± 0.4	119 ± 12	84 ± 14
2	5.5 ± 1.2	7 ± 0.6	119 ± 12	66 ± 4
3	5.0 ± 1.2	1.5 ± 0.3	131 ± 13	31 ± 10
4	5.0 ± 2.4	1 ± 0.3	121 ± 7	33 ± 7
5	6.0 ± 0.7	-	-	35 ± 9
6	-	-	-	< 10

Table 2: Paleomagnetic field values (mean and standard deviation) experienced by each region of cloudy zone for the four pallasites, calculated from pixel intensity histograms. Values for the Imilac and Esquel are taken from Bryson et al. (2015).

D. Solidification time for a magma ocean and the lifetime of an early thermal dynamo

Elkins-Tanton et al. (2011) argue that in order to generate a thermally driven core dynamo, a magma ocean is almost always required to generate the required heat flux across the core mantle boundary to drive vigorous convection. They assume that a core forms instantaneously upon 10 vol.% melting of the parent body. At this point the core is in thermal equilbrium with the magma ocean from which it has just differentiated. The pallasite parent body is assumed to have a radius of 200km (see Supplementary Section A), and hence forms a melt region with radius 92 km upon 10 vol.% melting of the body. Since the pallasite parent body has a final core of radius 100 km, it is assumed that the body is made up of ~12.5 vol.% metal (not including the metal that forms the pallasites, which is assumed to be injected during impact and is therefore not involved in initial accretion). Therefore it forms an initial core of radius 46 km, overlain by a magma ocean with depth 46 km.

The time taken for this magma ocean to solidify can be considered simply as a Stefan problem. We consider top-down solidification of the magma ocean, where latent heat is liberated from the solidification boundary by vertical conduction. The solidification boundary propagates downwards, until the entire magma ocean has solidified. The time for magma ocean solidification is given by:

$$t = \frac{y_m^2}{4\lambda_1^2 \kappa}$$

where y_m= 46 km, the depth of the magma ocean in the pallasite parent body. $\varkappa$, the thermal diffusivity is taken to be 1 mm^2s^{-1}. λ_1 can be solved iteratively using the following equation

$$\frac{L\sqrt{\pi}}{c(T_m - T_o)} = \frac{e^{-\lambda_1^2}}{\lambda_1 \lambda_1}$$

Where L, latent heat, is assumed to be 320 $kJkg^{-1}$ and c, specific heat, is assumed to be 1 $kJkg^{-1}$. T_m is the melting point of the mantle, which is assumed to be 1500 K (approximate melting point of dunite) and the temperature at the surface, T_o, is 250 K (Bryson et al. 2015).

This gives a magma ocean duration of $\sim$ 17 Ma. This value is an overestimate, since it does not account for convective heat loss in the solid lid, or heat transport by advection due to the presence of melts. This supports a very short-lived initial thermal dynamo on the pallasite parent body.

E. Derivation of Internal Field Strength

In order to test the likelihood of a weak magnetic field generated by a crustal remanence, we used Runcorn's theorem (Runcorn, 1975) to calculate the magnitude of an internal magnetic field generated by a crustal remanence, assuming an idealised, spherical body with a crust of uniform thickness that was magnetised by a dipolar field. The internal uniform field, which the pallasites are assumed to have sampled, is parallel to the axis of magnetisation of the crust, with an intensity of $4\pi/3$ times the maximum intensity of the magnetisation at the surface, multiplied by

the ratio of the magnetised to unmagnetised proportions of the body. The maximum magnetic field at the surface is given by

$$B_{max} = \frac{\mu_0 M_{dyn}}{2\pi r^3} \tag{1}$$

where M_{dyn} is the magnetic moment of the core dynamo, r is the radius of the body and μ_0 is the magnetic permeability of free space. The ratio of magnetised to unmagnetised proportions of the body are given by the ratio of crustal volume over the interior volume

$$\frac{V_{magnetised}}{V_{unmagnetised}} = \frac{(r^3 - r_1^3)}{r_1^3} \tag{2}$$

where r - r_1 gives the magnetic crustal thickness (r is the radius of the body and $r_1$is the distance from the centre of the body to the base of the magnetic crust), calculated from the thermal model for the MG pallaite parent body, based on the Curie temperature of a range of magnetic phases (Figure 3).

The nature and abundance of crustal magnetic material also needs to be taken into account. This is entirely unknown, so is calculated for hematite, magnetite, tetrataenite and pure Fe, for a range of wt% using empirically measured magnetisation values for each material (Kletetschka et al., 2006) to calculate their respective magnetic susceptibilites (χ_{TRM}) which are unitless for SI units (Table 3). The magnetic susceptibility depends on the type and amount of each magnetic phase present in the crust, assuming an average crustal density of 3200 kg m^{-3} (Johnson et al., 2015).

$$\chi_{TRM} = \frac{M \rho_{crust} f_i}{B/\mu_o} \tag{3}$$

where M represents the magnetisation in Am^2 kg^{-1}in a given field, B, and f_i is the fraction of magnetic material in the crust. The maximum magnetisation at the surface can then be calculated using

$$M_{TRM} = \frac{\chi_{TRM} B_{max}}{\mu_o} \tag{4}$$

Runcorn's theorem is then used to calculate the internal magnetic field, $B_{internal}$

$$B_{internal} = \mu_o \left(\frac{4\pi}{3} \frac{(r^3 - r_1^3)}{r_1^3} M_{TRM} \right) \tag{5}$$

Since we are only considering thin crust, this expression can be simplified to

$$B_{internal} = 4\pi\mu_o \frac{t_{crust}}{r} M_{TRM} \tag{6}$$

where t_{crust} is the crustal thickness and r, the radius of the MG pallasite parent body is taken to be 200 km.

The moment of a thermally driven core dynamo is predicted to be $\sim 10^{16}$ A m^2, two orders of magnitude less than that predicted for a compositional dynamo (Bryson et al., 2015; Olson and Christensen, 2006). The magnetic susceptibility of the crust is varied from 0 to 100, to account for a crust with up to 100 wt% tetrataenite or Fe, 25 wt% magnetite or 10 wt% hematite. Crustal thickness is varied from 0 to 20 km; 20 km is predicted to be the maximum thickness of material that would have cooled through its Curie temperature and become magnetised during the expected duration of the thermally driven core dynamo. This thickness provides an upper bound, since further cooling is required for the magnetic phases to reach their blocking temperature and lock in a thermal remanent magnetisation (TRM) (Figure 3).

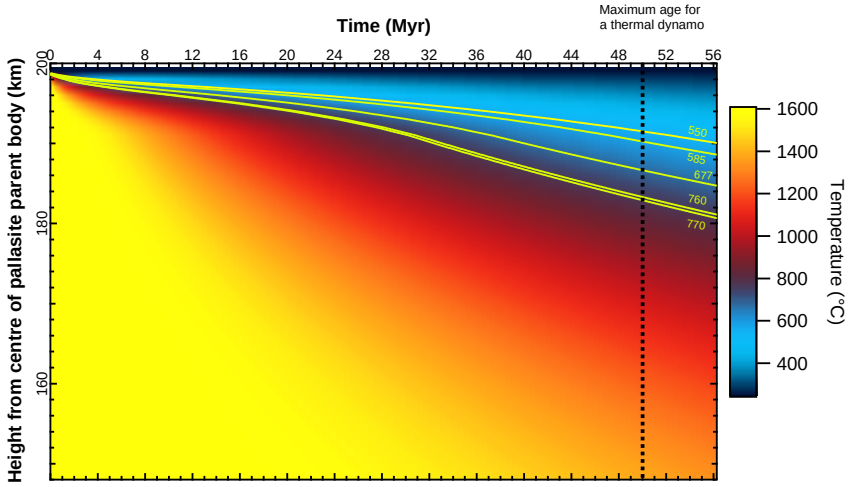

Figure 3: Crustal thickness calculated up until the maximum age for a thermal dynamo using a cooling model developed by Bryson et al. (2015). Contours represent the curie temperature of several different possible magnetic phases which may be present in the crust: tetrataenite $T_C = 550$ °C, magnetite $T_C = 585$ °C, hematite $T_C = 677$ °C, kamacite $T_C = 760$ °C, pure Fe $T_C = \tilde{}770$ °C which gives a maximum bound on the crustal thickness of ~ 20 km.

Applied External Field	Susceptibility (SI)			
(nT)	Fe	FeNi	Magnetite	Hematite
4.0×10^{-8}	3.44×10^{-4}	2.15×10^{-4}	3.52×10^{-3}	6.10×10^{-3}
8.0×10^{-8}	3.87×10^{-4}	2.68×10^{-4}	4.48×10^{-3}	2.10×10^{-2}
1.6×10^{-7}	6.36×10^{-4}	1.86×10^{-4}	5.22×10^{-3}	2.06×10^{-2}
3.5×10^{-7}	3.07×10^{-4}	2.72×10^{-4}	4.21×10^{-3}	1.06×10^{-2}
5.5×10^{-7}	6.53×10^{-4}	1.91×10^{-4}	4.05×10^{-3}	6.15×10^{-3}
1.6×10^{-6}	6.34×10^{-4}	1.86×10^{-4}	4.95×10^{-3}	1.68×10^{-2}
2.6×10^{-6}	6.23×10^{-4}	4.49×10^{-4}	4.89×10^{-3}	2.94×10^{-2}
6.0×10^{-6}	2.21×10^{-3}	6.97×10^{-4}	3.84×10^{-3}	4.97×10^{-2}
1.2×10^{-5}	2.75×10^{-3}	1.62×10^{-3}	1.14×10^{-2}	1.31×10^{-1}
2.4×10^{-5}	4.98×10^{-3}	3.37×10^{-3}	1.75×10^{-2}	2.02×10^{-1}
4.8×10^{-5}	1.32×10^{-2}	7.01×10^{-3}	2.38×10^{-2}	2.60×10^{-1}
9.8×10^{-5}	2.16×10^{-2}	1.29×10^{-2}	5.81×10^{-2}	3.20×10^{-1}

Table 3: Magnetic susceptibility is calculated for Fe, FeNi, Magnetite and Hematite using the mean of the reported values of TRM Kletetschka et al. (2006). Susceptibility is dimensionless, and calculated in SI units.

Bryson, J. F. J., Nichols, C. I. O., Herrero-Albillos, J., Kronast, F., Kasama, T., Alimadadi, H., Laan, G. V. D., Nimmo, F., Harrison, R. J., 2015. Long-lived magnetism fromo solidification-driven convection on the pallasite parent body. Nature 517 (7535), 472–475.
URL `http://dx.doi.org/10.1038/nature14114`

Elkins-Tanton, L. T., Weiss, B. P., Zuber, M. T., may 2011. Chondrites as samples of differentiated planetesimals.

Earth and Planetary Science Letters 305 (1-2), 1–10.
URL http://linkinghub.elsevier.com/retrieve/pii/S0012821X11001543

Johnson, C. L., Phillips, R. J., Purucker, M. E., Anderson, B. J., Byrne, P. K., Denevi, B. W., Feinberg, J. M., Hauck, S. a., Head, J. W., Korth, H., James, P. B., Mazarico, E., Neumann, G. a., Philpott, L. C., Siegler, M. a., Tsyganenko, N. a., Solomon, S. C., 2015. Low-altitude magnetic field measurements by MESSENGER reveal Mercury's ancient crustal field. Science (May), 1–36.
URL http://www.sciencemag.org/cgi/doi/10.1126/science.aaa8720

Kletetschka, G., Fuller, M. D., Kohout, T., Wasilewski, P. J., Herrero-Bervera, E., Ness, N. F., Acuna, M. H., 2006. TRM in low magnetic fields: A minimum field that can be recorded by large multidomain grains. Physics of the Earth and Planetary Interiors 154 (3-4), 290–298.

Olson, P., Christensen, U. R., 2006. Dipole moment scaling for convection-driven planetary dynamos. Earth and Planetary Science Letters 250 (3-4), 561–571.

Runcorn, S., 1975. On the interpretation of lunar magnetism. Physics of the Earth and Planetary Interiors 10 (4), 327–335.